# PICTURE OF THE MONTH

## Observed Inner-Core Structural Variability in Hurricane Dolly (2008)*

ERIC A. HENDRICKS

*Marine Meteorology Division, Naval Research Laboratory, Monterey, California*

BRIAN D. MCNOLDY

*Rosenstiel School of Marine and Atmospheric Science, University of Miami, Miami, Florida*

WAYNE H. SCHUBERT

*Colorado State University, Fort Collins, Colorado*

(Manuscript received 17 January 2012, in final form 22 June 2012)

ABSTRACT

Hurricane Dolly (2008) exhibited dramatic inner-core structural variability during a 6-h rapid intensification and deepening event just prior to making landfall in southern Texas at 1800 UTC 23 July. In particular, the eyewall was highly asymmetric from 0634–1243 UTC, with azimuthal wavenumber $m = 4$–7 patterns in the eyewall radar reflectivity and prominent mesovortex and polygonal eyewall signatures. Evidence is presented that the most likely cause of the high-wavenumber asymmetries is a convectively modified form of barotropic instability of the thin eyewall potential vorticity ring. The rapid intensification and deepening event occurred while Dolly was in a favorable environment with weak deep-layer vertical wind shear and warm sea surface temperatures; however, the environmental conditions were becoming less favorable during the period of rapid intensification. Therefore, it is plausible that the internal vortex dynamics were dominant contributors to the rapid intensification and deepening.

### 1. Introduction

One of the most important unsolved problems in tropical meteorology today is tropical cyclone (TC) intensity variability, including rapid intensification. It is widely known that TC intensity change is caused by environmental, oceanic, and internal dynamical factors (Wang and Wu 2004). One such important internal process is the dynamic instability of the eyewall potential vorticity (PV) annulus, its breakdown, and subsequent eddy flux of PV from the eyewall into the eye. This instability is more common in hurricanes (i.e., TCs with maximum sustained surface winds greater than 64 kt) because the radial profile of PV typically has a maximum in the eyewall region, where PV is continually produced by diabatic heating. The barotropic or combined barotropic–baroclinic instability of the eyewall and subsequent mixing has been a topic of much recent interest (Schubert et al. 1999; Kossin and Schubert 2001; Kossin and Eastin 2001; Montgomery et al. 2002; Terwey and Montgomery 2002; Kossin et al. 2002; Nolan and Montgomery 2002; Nolan and Grasso 2003; Kossin and Schubert 2004; Kwon and Frank 2005; Rozoff et al. 2009; Hendricks et al. 2009; Hendricks and Schubert 2010).

Detailed observations of the inner-core evolution of TCs have been sparse because TCs generally exist over the open oceans. However, on aircraft reconnaissance missions, airborne radar data have shown that significant variability can exist in the eyewall region (Marks et al. 1992; Reasor et al. 2000; Roux and Viltard 2004). Rarely are land-based Doppler radars able to capture intricate

* Supplemental information related to this paper is available at the Journals Online website: http://dx.doi.org/10.1175/MWR-D-12-00018.s1.

*Corresponding author address:* Eric A. Hendricks, Marine Meteorology Division, Naval Research Laboratory, 7 Grace Hopper Ave., Monterey, CA 93943.
E-mail: eric.hendricks@nrlmry.navy.mil

DOI: 10.1175/MWR-D-12-00018.1

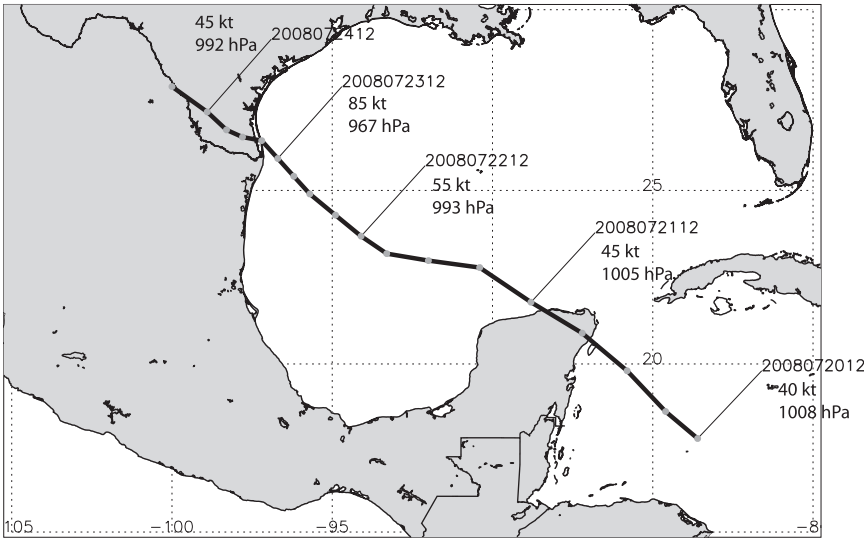


FIG. 1. The track of Hurricane Dolly. Each gray dot is 6 h apart. The NHC best-track intensity is also given at a number of date–time groups.

structural details of organized eyewalls, because the hurricane typically becomes disorganized as it approaches the coast, and second because there is a relatively short window of time prior to landfall that the storm is in radar range. Such a rare event occurred in 2008, as Hurricane Dolly approached the Texas coast. Unprecedented observations of the inner core of Dolly were taken from the National Weather Service Weather Surveillance Radar-1988 Doppler (WSR-88D) in Brownsville, Texas, prior to landfall. The observations showed a dynamic eyewall with significant azimuthal variability on short times scales (30 min to 1 h) during a 6-h rapid intensification and deepening period before it made landfall. The purpose of this note is to document this dramatic variability and to understand its role in the intensity variability of Dolly prior to landfall. This note is organized as follows. A brief synoptic history of Dolly is provided in section 2. An environmental analysis is provided in section 3. Analysis of the observed inner-core structural variability, along with numerical model simulations, are given in section 4. A summary is provided in section 5.

## 2. Synoptic history

The synoptic history of Dolly is provided by Pasch and Kimberlain(2011), and the track is given in Fig. 1. Dolly's origin can be traced to a tropical wave exiting Africa on 11 July 2008; however, it did not form into a tropical storm until 20 July, when it was in the western Caribbean Sea. After crossing the Yucatan peninsula at 1200 UTC 21 July, it moved westward toward southern Texas and slowed down. Dolly made landfall in South Padre Island at 1800 UTC 23 July as a category-1 hurricane with maximum winds of 75 kt (1 kt = 0.5144 m $s^{-1}$). After landfall, Dolly weakened and moved along the Texas and Mexico border.

The National Hurricane Center (NHC) best-track intensity estimates are shown in Fig. 2. These intensity estimates are based in part upon multiple aircraft reconnaissance missions that were conducted in Dolly from both the National Oceanic and Atmospheric Administration (NOAA) WP-3D and the U.S. Air Force (USAF) Reserve 53rd Weather Reconnaissance Squadron WC-130J aircraft. The vertically oriented solid black line indicates the landfall time, and the gray-shaded area indicates the period of significant eyewall asymmetries,

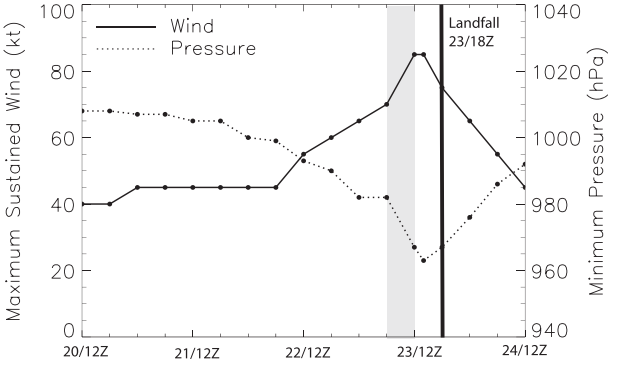


FIG. 2. Intensity of Hurricane Dolly by maximum sustained wind and minimum central pressure. The landfall time is marked by the solid black line and the gray-shaded area denotes the time period with dramatic eyewall structural variability. Note the extra observation at 1400 UTC 23 Jul from the U.S. Air Force WC-130J reconnaissance aircraft.

which is the focus of this note. Prior to 1200 UTC 22 July, Dolly had a steady intensity of approximately 40–45 kt. From 1200 UTC 22 July until approximately 1400 UTC 23 July, Dolly experienced rapid intensification, during which the maximum sustained wind increased from 45 to 85 kt, and the minimum pressure fell from 990 to 965 hPa. A significant portion of this rapid intensification occurred in the 6-h time frame between 0600 and 1200 UTC 23 July (gray-shaded area). In this short time period the maximum sustained winds increased from 70 to 85 kt, and the pressure fell from 982 to 963 hPa. The rapid intensification event occurred just prior to Dolly making landfall in southern Texas.

## 3. Environmental analysis

To help understand the relative roles of the internal and environmental processes in the rapid intensification and deepening of Dolly prior to landfall, analysis of the environmental conditions in the vicinity of Dolly are presented here. Four critical environmental parameters for tropical cyclone intensity change are the deep-layer vertical wind shear, sea surface temperature (SST), low- to midlevel relative humidity, and upper-level divergence. A brief review of how each of these factors modulates TC intensity is discussed in section 2c of Hendricks et al. (2010), and a more extensive review is provided by Wang and Wu (2004). These environmental parameters were obtained from the Statistical Hurricane Intensity Prediction System (SHIPS) database (DeMaria et al. 2005) during the period just prior to landfall. The atmospheric parameters are calculated using the Global Forecast System (GFS) operational analysis. The SHIPS database parameters used were (i) SHRD: magnitude of the deep-layer 850–200-hPa shear vector averaged from $r = 200$ to 800 km, (ii) RSST: Reynolds analysis sea surface temperature (Reynolds and Smith 1993), (iii) D200: 200-hPa divergence averaged from $r = 0$ to 1000 km, and (iv) RHMD: 700–500-hPa relative humidity averaged from $r = 200$ to 800 km.

The deep-layer shear and SST are plotted in Fig. 3a from 1200 UTC 22 July to 0000 UTC 24 July. The period of eyewall asymmetries (and rapid intensification and deepening) is shaded in light gray. It can be seen that the shear was increasing prior to 0600 UTC 23 July, reaching a value of 6 m $s^{-1}$ during the period of eyewall asymmetries. The average sea surface temperature gradually became cooler from 1200 UTC 22 July to 0000 UTC 24 July, decreasing from 29.2° to 27.9°C. The upper-level divergence and midlevel relative humidity are plotted in Fig. 3b. As shown by Fig. 3b, from 0000 to 1200 UTC 23 July, the upper-level divergence decreased significantly, from $4.7 \times 10^{-6}$ to $1.0 \times 10^{-6}$ $s^{-1}$. The average low- to midlevel relative humidity decreased from 0000 to 0600 UTC 23 July (from 67% to 62%), then increased from 0600 to 1200 UTC 23 July (from 62% to 69%). Synthesizing the above results, the environment was very favorable for intensification between 1200 UTC 22 July and 0000 UTC 23 July. The SSTs were greater than 29°C, the deep-layer shear was approximately 3 m $s^{-1}$, and strong upper-level divergence existed. The environment became less favorable from 0000 to 1200 UTC 23 July. The SSTs decreased to 28.9°C on average, the deep-layer shear increased to 6 m $s^{-1}$, and the upper-level divergence decreased significantly.

During the period of interest here (gray-shaded area of Figs. 3a and 3b), when Dolly was rapidly intensifying and deepening with prominent eyewall asymmetries, the environmental conditions were generally becoming less favorable. From the four important environmental parameters examined, all except the midlevel relative humidity were becoming less favorable for intensification. Therefore, it is possible that the rapid intensification and deepening event may have been more strongly controlled by the vortex internal dynamics than the environmental conditions for this case. This is explored in the next section.

## 4. Inner-core analysis

### a. Observed eyewall evolution

The observed inner-core evolution of Dolly was captured by the National Weather Service Doppler radar located in Brownsville, Texas (station identifier: KBRO). In Fig. 4, the base radar reflectivity from KBRO is shown from 0400 to 1400 UTC 23 July, which is during the rapid intensification and deepening event. Radar images are shown every 2 h, and a time series of best-track intensity (red line) and central pressure (blue line) is plotted above each panel, with the time corresponding to the radar image denoted by a vertical green line. In Fig. 4a, Dolly is just coming into view of the radar. By 0600 UTC (Fig. 4b), some eyewall asymmetries can be seen in the reflectivity, particularly on the northern portion of the eyewall. By 0800 UTC (Fig. 4c), there is a high azimuthal wavenumber pattern in the eyewall (wavenumber 5 or 6). By 1000 UTC (Fig. 4d), the most prominent pattern has been reduced to wavenumber 4 or 5. At 1200 UTC (Fig. 4e), there is more variability on the southern part of the eyewall. Finally, by 1400 UTC (Fig. 4f), the inner-core of Dolly becomes more axisymmetric. There now exists a wavenumber-1 pattern in the reflectivity, with most of the deep convection on the southern side of the eyewall. As noted by Pasch and Kimberlain (2011), the opening of the eyewall on the northern semicircle at this time was a factor causing Dolly to weaken just prior to landfall, perhaps due to ingestion of drier air.

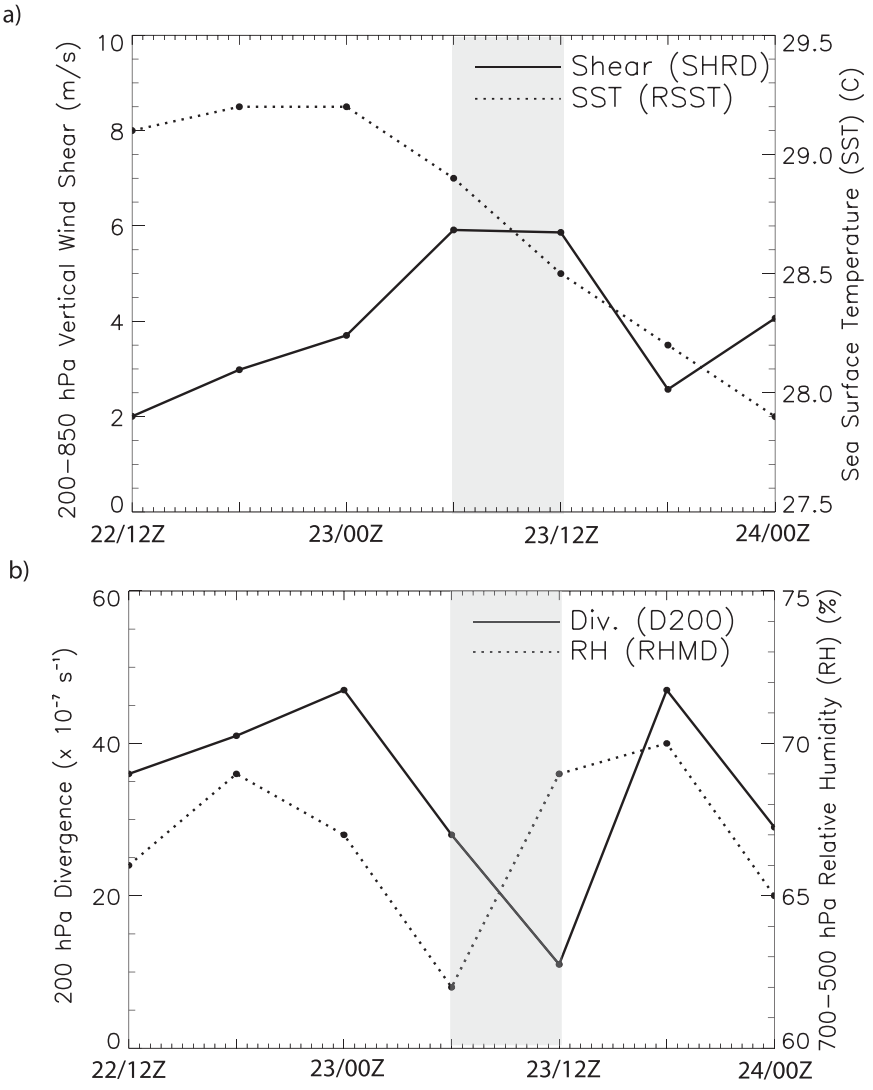


FIG. 3. Evolution of the environmental conditions in the vicinity of Dolly. (a) 200–850-hPa deep-layer wind shear magnitude and SST, and (b) 200-hPa divergence and 700–500-hPa relative humidity. The gray-shaded region denotes the period of eyewall asymmetries and rapid intensification and deepening.

A detailed view of Dolly's inner-core evolution is provided in Fig. 5. Here the evolution of Dolly's eyewall is provided at approximately 30-min intervals, from 0503 to 1433 UTC 23 July, during the rapid intensification event. The diameter of the eyewall is approximately 45–50 km (inferred from the radar data). Here structural variability on very short time scales can be seen (30 min to 1 h), with the eyewall vacillating between wavenumber-4–6 patterns. At many instances, the inner edge of the eyewall has small curved features (e.g., at 0900 UTC), resembling mesovortices. At other instances, straight-line segments and polygonal eyewalls can be seen. An interesting feature that can be seen in Fig. 5 is the evolution of the eyewall asymmetries from higher to lower azimuthal wavenumbers. From 0702 to 0943 UTC 23 July, the asymmetries are at azimuthal wavenumbers $m$ = 6–7. Subsequently from 0934 to 1234 UTC, the asymmetries are observed to be at lower azimuthal wavenumbers $m$ = 4–5. Finally, from 1234 to 1433 UTC, the eyewall is observed with a wavenumber $m$ = 1 pattern with the highest radar reflectivity on its southern portion. It is not known whether the high-wavenumber asymmetries evolve into lower-wavenumber asymmetries, or whether the high-wavenumber asymmetries grow first, decay, and then are followed by a slower-growing lower-wavenumber asymmetry. This phenomenon is of scientific interest and warrants further research.

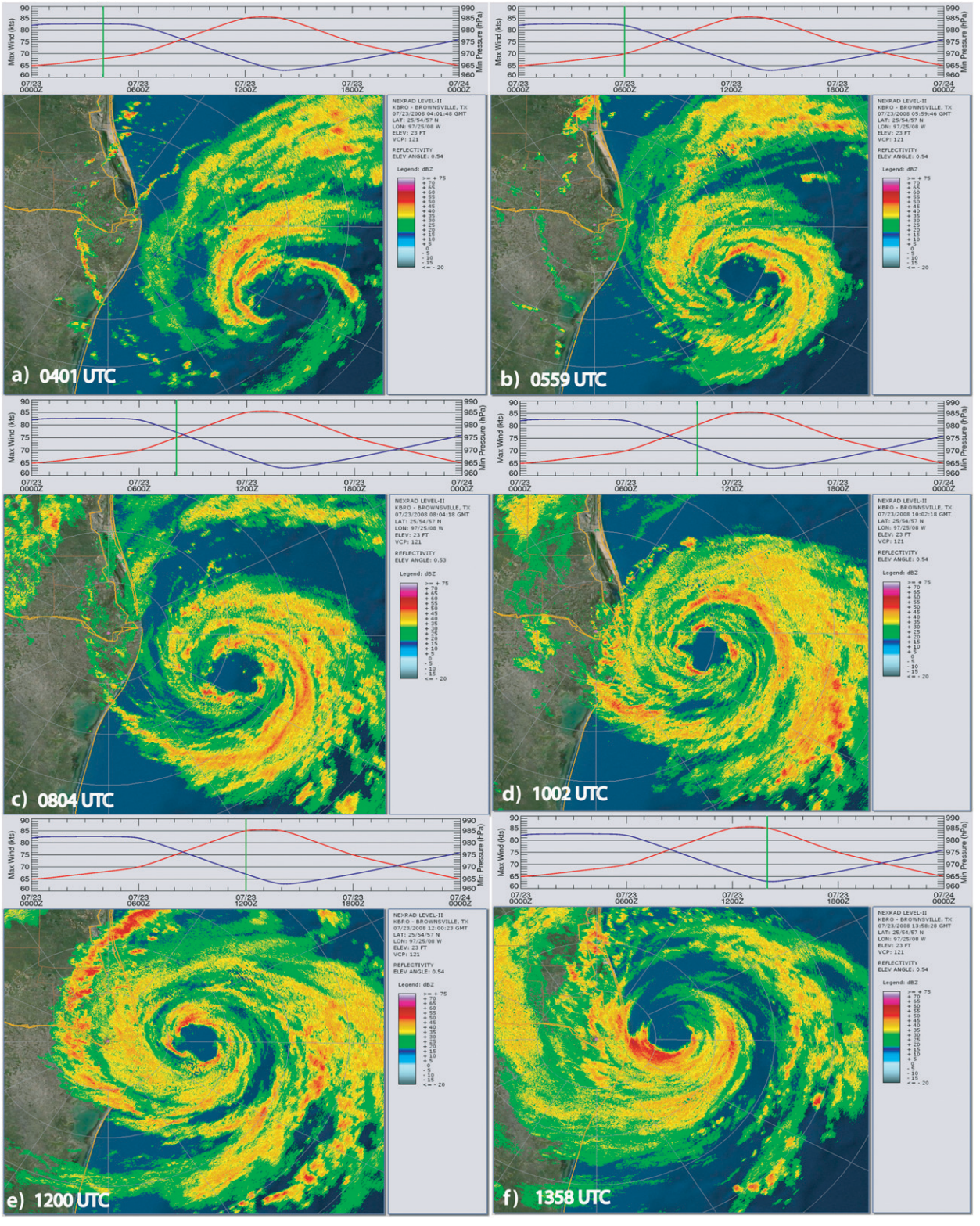


FIG. 4. Structural variability of Hurricane Dolly from the KBRO radar and associated intensity from NHC best-track data. The time of the image is indicated by the vertical green line on the intensity and pressure plot.

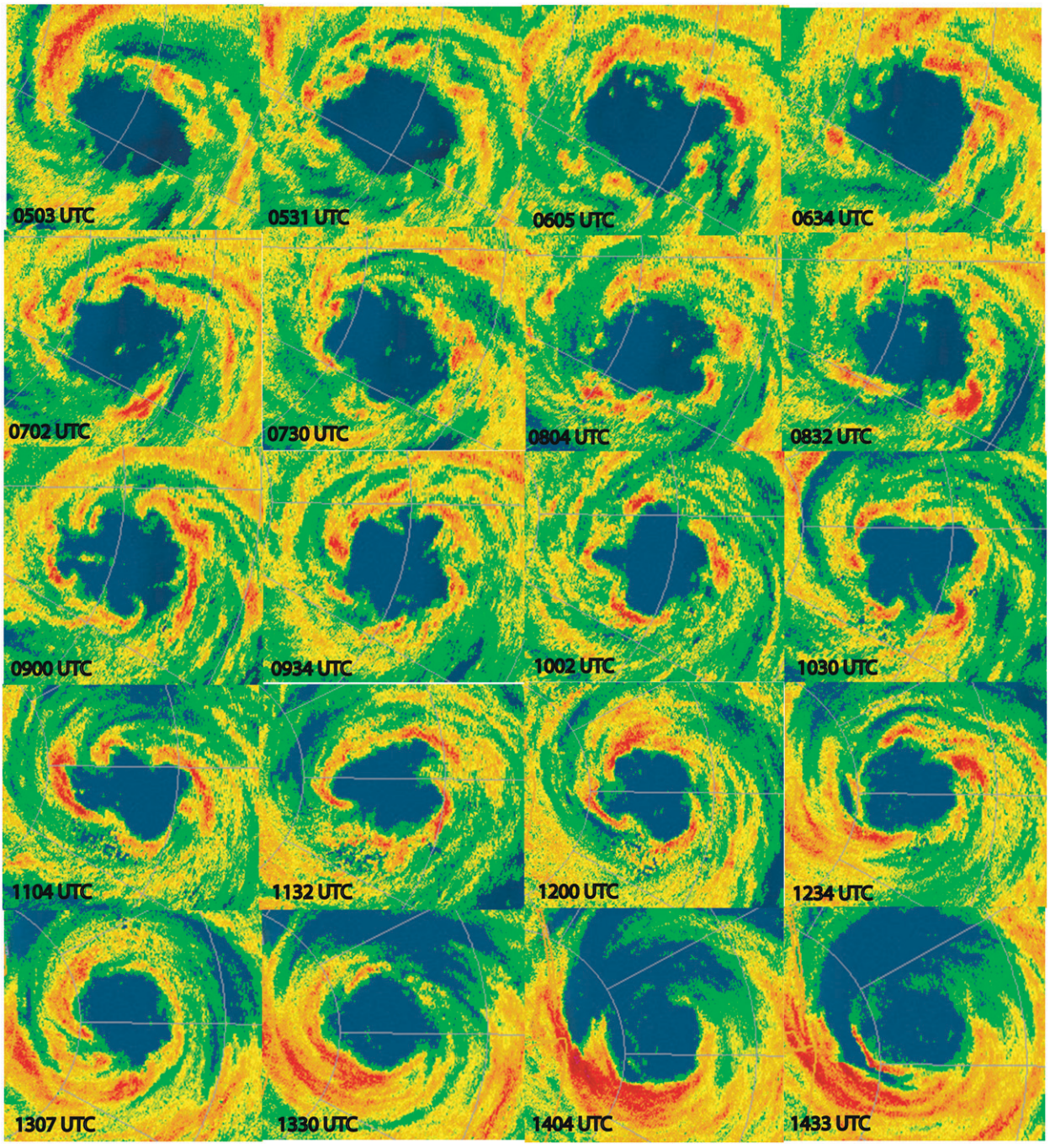


FIG. 5. Detailed temporal evolution of the eyewall of Hurricane Dolly. The first panel is at 0503 UTC 23 Jul, and each subsequent panel is approximately 30 min after the previous panel. Panels increase in time in the horizontal. The last panel is at 1433 UTC 23 Jul. The approximate diameter of the eyewall is 45–50 km.

In Fig. 6, the vertical structure of the inner core is shown at 1052 UTC 23 July. At this time, at low levels, there is a prominent wavenumber-4 pattern. The wavenumber-4 pattern exists to a height of approximately 4200 m (although it is not as pronounced as near the surface). Moving to upper levels (9800 m), the eyewall is more axisymmetric. This demonstrates that the asymmetries in the eyewall are primarily confined to lower levels during the instability. This observation is consistent with the three-dimensional numerical modeling results of Hendricks and Schubert (2010), who showed that unstable PV waves grow most rapidly at lower levels where

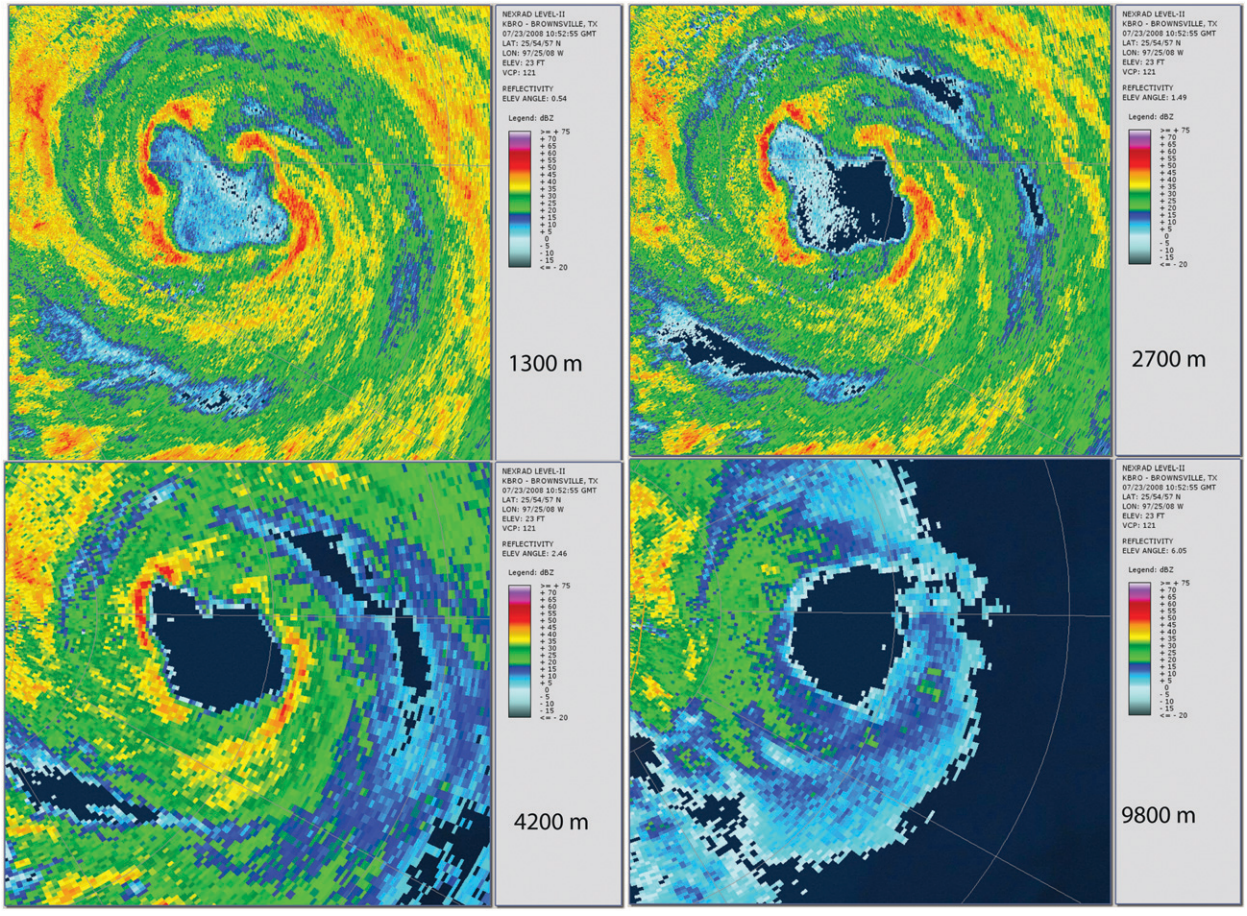


FIG. 6. Inner-core of Dolly as seen by KBRO at different vertical heights at 1052 UTC 23 Jul: 1300, 2700, 4200, and 9800 m.

the radial shear of the tangential velocity is largest (cf. Schubert et al. 1999). Another important feature to note is that the phases of the asymmetries are approximately the same from 1300 to 4200 m. There exists no apparent upshear tilt of the asymmetries in the vertical, which would signify that a baroclinic instability is occurring. Therefore, barotropic instability appears to be the dominant cause of the asymmetries in the Dolly case, and the entire hollow PV tower below 4200 m breaks down in unison. The following supplemental materials are also included to enhance the description of the eyewall evolution of Hurricane Dolly in this section: (i) radar animation with intensity, (ii) close-up animation of the eyewall, (iii) visible and infrared satellite animations, and (iv) seven vertical scans of the eyewall at 1052 UTC 23 July.

### *b. Aircraft reconnaissance data*

A U.S. Air Force WC-130J reconnaissance aircraft completed a mission into Dolly from 0800 to 2016 UTC 23 July. During the period of interest here, the aircraft completed three radial flight legs (from 1040 to 1230 UTC), shown in Fig. 7a. The flight level was 700 hPa and the data output was available every 10 s. The aircraft data were obtained from the NOAA/Atlantic Oceanographic and Meteorological Laboratory/Hurricane Research Division in Miami, Florida (http://www.aoml.noaa.gov/hrd/). The flight-level winds were used as a proxy to ascertain azimuthal mean characteristics of the tangential velocity and relative vorticity at lower levels (cf. Kossin and Eastin 2001).

In computing the relative vorticity, it was assumed that the winds measured on the flight legs were mostly tangential since the aircraft flew above the boundary layer directly through the vortex center. The data processing procedure is as follows. First, the aircraft position and measured wind speed were interpolated to a radial grid with the origin at the location of the minimum measured wind speed (the center of the eye). A five-point smoothing filter was applied to the raw winds to reduce high-frequency variability, effectively removing variability with horizontal wavelengths less than 5 km.

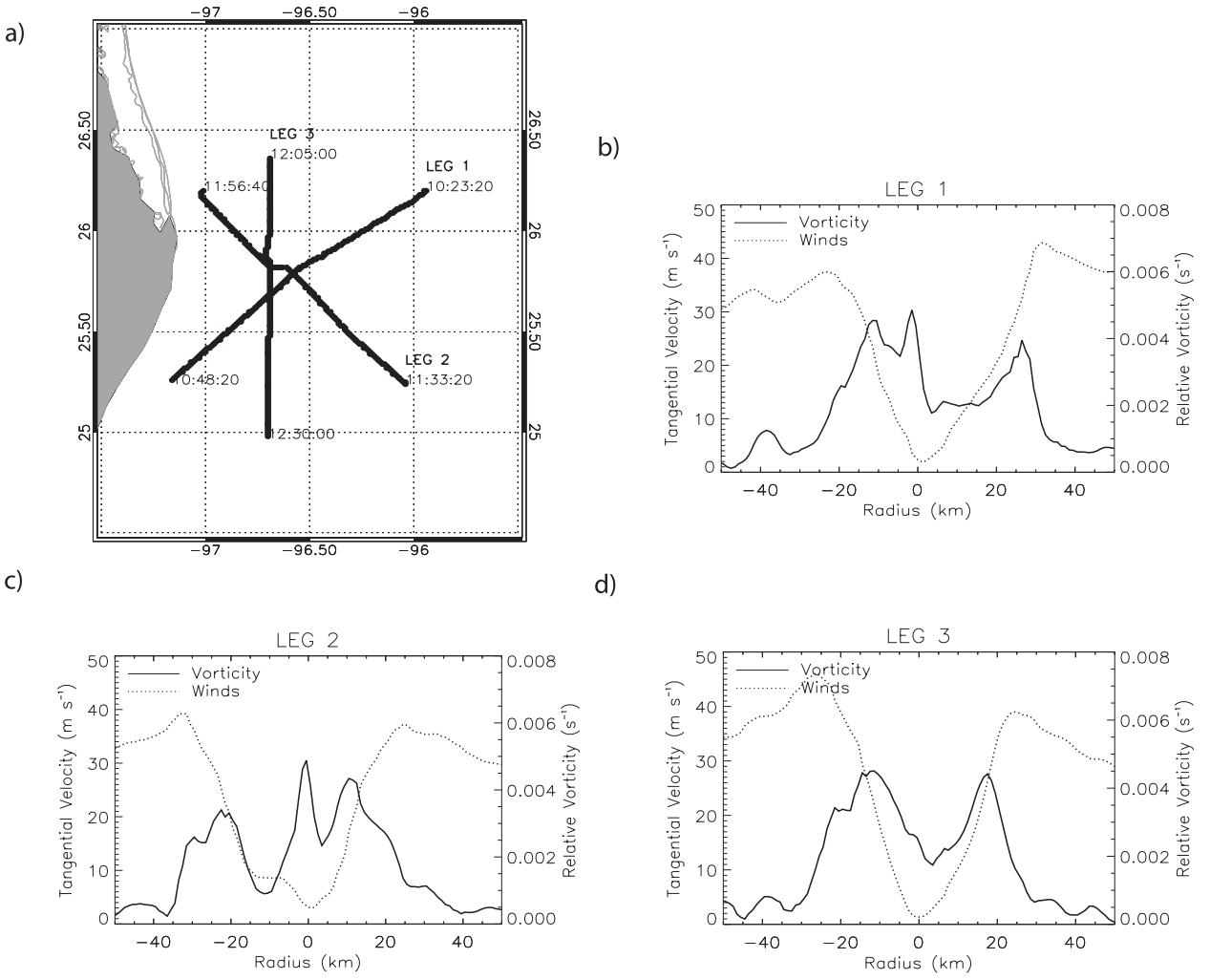


FIG. 7. (a) Radial flight legs from the U.S. Air Force WC-130J reconnaissance aircraft on 23 Jul. (b) Flight-level winds and relative vorticity from inner region of leg 1. (c) As in (b), but for leg 2. (d) As in (c), but for leg 3. Legs are centered on the recorded minimum wind speed by the WC-130J aircraft, and radii increase outward from the center.

For convenience of examining all legs in the same reference frame, while simplifying the inbound and outbound portion of each leg, increasing radii were set to denote moving across the TC on a given leg from left to right. Thus, for legs 1 and 2, increasing radii denotes moving across the leg backward in time, while for leg 3, the opposite is true. Next, the irregularly gridded flight-level winds were interpolated to a regular grid with spacing of $dr = 1$ km, which is similar to the average spacing of the irregular grid. Then, the relative vorticity was calculated using centered differencing of the winds on this regular grid [i.e., $\zeta_{i+1/2} = v_{i+1/2}/r_{i+1/2} + (v_{i+1} - v_i)/(r_{i+1} - r_i)$, where $r_{i+1/2} = (r_i + r_{i+1})/2$, and $v_{i+1/2} = (v_i + v_{i+1})/2$]. Finally, a three-point smoothing filter was applied to the relative vorticity to further reduce high-frequency variability, while retaining characteristics of the azimuthal mean vorticity.

In Figs. 7b–d, both the flight-level winds and relative vorticity are given in the inner region of each flight leg. Examining the winds in leg 1 in Fig. 7b, the eye diameter of Dolly is approximately 50 km. The relative vorticity exhibits a thin and moderately hollow profile (i.e., a thin vorticity ring with maximum vorticity in the eyewall and some vorticity in the eye) to the northeast of the center and more Rankine-like to the southwest. Peak winds and vorticity at this time are approximately 40 m $s^{-1}$ and 0.005 $s^{-1}$, respectively. Moving to leg 2 (Fig. 7c), the relative vorticity exhibits a more hollow profile to the southeast and more Rankine-like to the northwest. Finally, by leg 3 (Fig. 4d), the winds have increased to 45 m $s^{-1}$, and the relative vorticity has a hollow profile across the eye, moving from north to south. At this time, the eye diameter has decreased slightly to 45 km.

During this reconnaissance mission, Dolly was undergoing dramatic inner-core structural variability, as shown by Fig. 5. The time period of leg 1 corresponds to the 1030 UTC image, the time period of leg 2 corresponds to the 1132/1200 UTC images, and the time period of leg 3 corresponds to the 1200/1234 UTC images. Overall, the reconnaissance data indicated that the relative vorticity exhibited variation from moderately hollow to Rankine-like radial profiles. Since the Rayleigh necessary condition for barotropic instability was satisfied on some portions of the radial legs (i.e., the radial vorticity gradient changes sign), and considering the morphology of the radar reflectivity depicted in Figs. 4 and 5, it is very likely that the cause of the asymmetries in Dolly was dynamic instability of its thin vorticity ring. This is explored through numerical simulations in section 4c.

*c. Numerical simulations*

To confirm that the origin of the Dolly asymmetries was dynamic instability of the eyewall, numerical simulations were conducted with a shallow-water model. Although the shallow-water model is an oversimplification of the real atmosphere, it is a useful starting point to understand barotropic instability and advective dynamics. The numerical model is based on the vorticity-divergence formulation of the shallow-water equations:

$$\frac{\partial \delta}{\partial t} + \nabla \cdot \{(f+\zeta)\mathbf{k} \times \mathbf{u}\} + \nabla^2\left(gh + \frac{1}{2}\mathbf{u}\cdot\mathbf{u}\right) = 0, \quad (1)$$

$$\frac{\partial \zeta}{\partial t} + \nabla \cdot \{(f+\zeta)\mathbf{u}\} = 0, \quad (2)$$

$$\frac{\partial h}{\partial t} + \nabla \cdot \{(\overline{h}+h)\mathbf{u}\} = 0, \quad (3)$$

where $\mathbf{u}$ is the horizontal velocity vector, $f$ is the constant Coriolis parameter, $\mathbf{k}$ is the vertical unit vector, $\zeta = \mathbf{k} \cdot \nabla \times \mathbf{u}$ is the relative vorticity, $\delta = \nabla \cdot \mathbf{u}$ is the divergence, $g$ is the acceleration of gravity, and $h$ is the deviation of the free surface height from the constant mean value $\overline{h} = 6371$ m.

The solutions presented here were obtained with a double Fourier pseudospectral discretization, using a 600 km × 600 km domain with 512 × 512 points. After dealiasing of the quadratic advection terms, 170 Fourier modes were kept, yielding an effective resolution of 3.52 km. To control spectral blocking, ordinary $\nabla^2$ diffusion terms were included on the right-hand sides of the prognostic equations (1)–(3). The numerical diffusion coefficient was set to 25 $m^2\ s^{-1}$. Time differencing was accomplished using a third-order explicit scheme with a time step of 4 s. The constants in (1)–(3) were chosen to be $f = 3.7 \times 10^{-5}\ s^{-1}$ and $(g\overline{h})^{1/2} = 250\ m\ s^{-1}$.

An initial condition of a thin vorticity ring was constructed in accordance with the flight-level vorticity of leg 1 from $r = 0$ to 30 km. The initial condition was defined mathematically by

$$\overline{\zeta}(r,0) = \begin{cases} \zeta_1 & 0 \le r \le r_1 \\ \zeta_1 S\left(\dfrac{r-r_1}{r_2-r_1}\right) + \zeta_2 S\left(\dfrac{r_2-r}{r_2-r_1}\right) & r_1 \le r \le r_2 \\ \zeta_2 & r_2 \le r \le r_3, \\ \zeta_2 S\left(\dfrac{r-r_3}{r_4-r_3}\right) + \zeta_3 S\left(\dfrac{r_4-r}{r_4-r_3}\right) & r_3 \le r \le r_4 \\ \zeta_3 & r_4 \le r < \infty \end{cases} \quad (4)$$

where $\zeta_1$, $\zeta_2$, $\zeta_3$, $r_1$, $r_2$, $r_3$, and $r_4$ are constants, and $S(s) = 1 - 3s^2 + 2s^3$ is a cubic Hermite shape function that provides smooth transition zones. The eyewall is defined as the region between $r_2$ and $r_3$, and the transition zones are defined as the regions between $r_1$ and $r_2$, and $r_3$ and $r_4$. Here $\zeta_1 = 2.0 \times 10^{-3}\ s^{-1}$, $\zeta_2 = 5.0 \times 10^{-3}\ s^{-1}$, $r_1 = 15$ km, $r_2 = 19$ km, $r_3 = 23$ km, and $r_4 = 27$ km. Here $\zeta_3$ was set to a small negative number so the circulation is zero at the boundaries. The ring was constructed such that the maximum tangential velocity was set to 40 $m\ s^{-1}$ (77 kt), consistent with the Dolly observations during its structural variability phase. To initiate the instability process, a broadband perturbation was added to the basic-state vorticity. The initial $h$ field was determined by solving the nonlinear balance equation, and the initial $\delta$ field was set to zero. Schubert et al. (1999) used two parameters to define hurricane-like vorticity rings: the hollowness parameter $\gamma = \zeta_1/\zeta_{av}$ (where $\zeta_{av} = 0.0036\ s^{-1}$ is the average inner-core vorticity) and the thickness parameter, denoted here as $\alpha = (r_1 + r_2)/(r_3 + r_4)$. For this ring $\gamma = 0.72$ and $\alpha = 0.67$, which according to barotropic theory and idealized simulations is most unstable to azimuthal wavenumbers 5–6 (Schubert et al. 1999; Hendricks et al. 2009).

The evolution of the potential vorticity $P = \overline{h}(f+\zeta)/h$ for the experiment is given in Fig. 8. By $t = 2.5$ h, the most unstable mode of azimuthal wavenumber 5 begins to become visible and grows by $t = 3.75$ h. Finally, by $t = 5.0$ h and $t = 6.25$ h, the wavenumber-5 pattern becomes more prominent. The numerical simulation confirms that barotropic instability of a vortex with Dolly's observed radial vorticity profile (from the WC-130J aircraft) can produce the high azimuthal wavenumber asymmetric variability of similar structure and on similar time scales that were observed (Fig. 4). Therefore, it is most plausible that the asymmetries depicted in Dolly

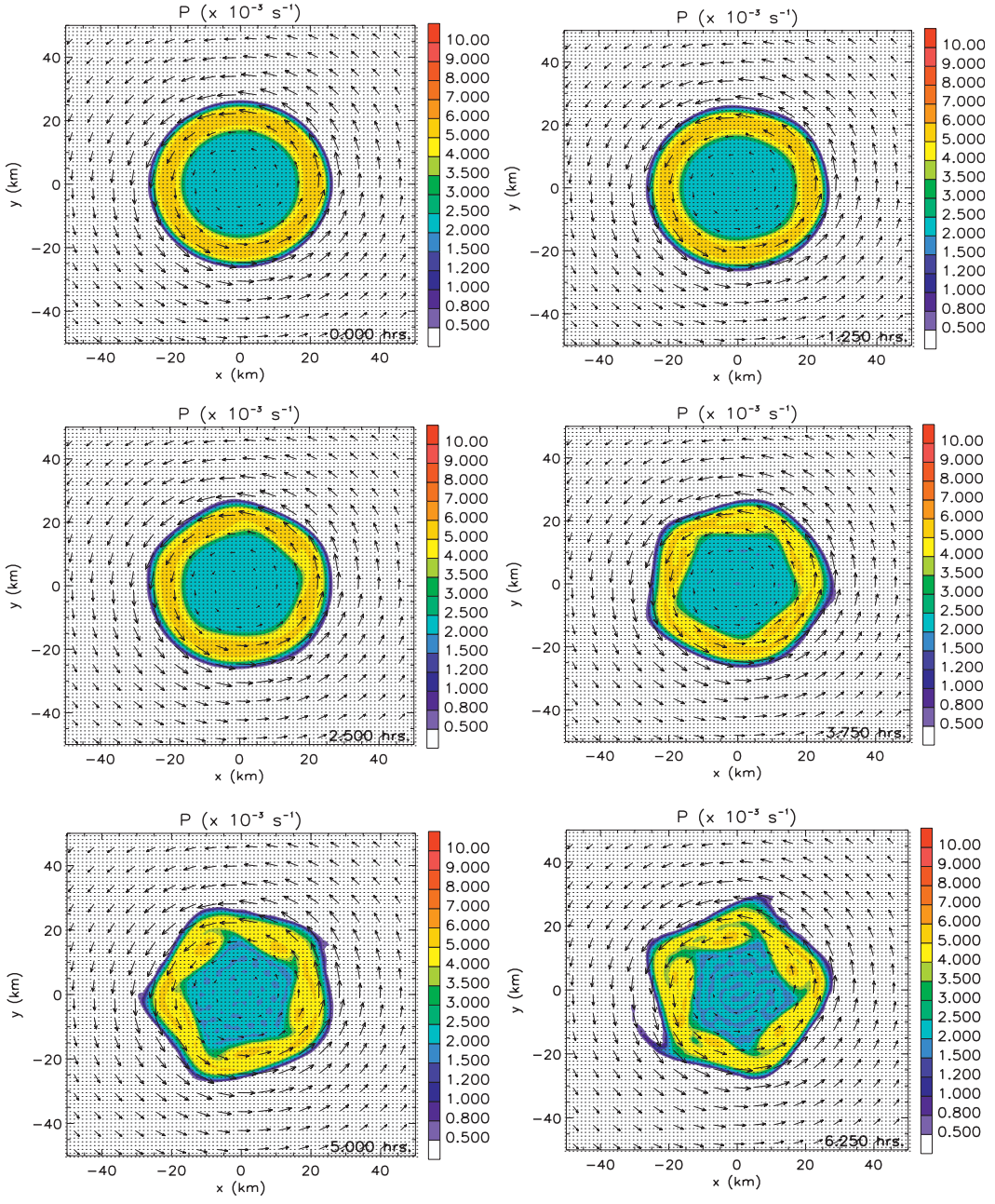


FIG. 8. Evolution of the PV ring matching Dolly's radial vorticity profile for leg 1 in the shallow-water model. Only the inner 100 km × 100 km of the 600 km × 600 km domain is shown.

were a result of barotropic instability of its thin potential vorticity ring.

### *d. Discussion*

We have documented significant inner-core structural variability observed in Hurricane Dolly during a rapid intensification and deepening event from 0600 to 1200 UTC 23 July 2008. It has been shown that the most likely cause of the high-wavenumber asymmetries is a convectively modified form of dynamic instability of a thin potential vorticity ring. In the context of balanced dynamics, previous idealized modeling work has shown that when dry unstable barotropic vortices break down, both the minimum pressure and maximum sustained wind simulaneously decrease (Schubert et al. 1999; Kossin and Schubert 2001; Hendricks et al. 2009; Hendricks and Schubert 2010). The reduction in pressure occurs because the asymmetric mixing of high PV air from the eyewall

into the eye increases the centrifugal term in the gradient wind balance equation, while the reduction in tangential velocity happens because the PV is fluxed from the eyewall into the eye, reducing the winds in the eyewall. While the dry barotropic-balanced dynamics explains a portion of the reduction in minimum surface pressure in Dolly, the increase in low-level winds cannot be explained by this mechanism. It is possible that diabatic effects could have combined with the dry dynamics to create an increase in low level PV (and therefore the low-level winds) for this case. However, there are many more complicating factors of how this process proceeds in the real atmosphere. For example, in full-physics numerical simulations, Yang et al. (2007) found that the net effect of the asymmetries was to reduce the maximum intensity of the cyclone (cf. an axisymmetric simulation) through a thermodynamic mechanism where downdraft cooling and drying effects were limited, leading to reduced surface fluxes underneath the eyewall. In contrast to this, Chen and Yau (2001) found that inward PV mixing caused intensification of the hurricane. Clearly, the interaction of convective and dynamic instabilities as well as their relationship to tropical intensity variability, deserve further research in a hierarchy of numerical modeling frameworks.

## 5. Summary

Hurricane Dolly (2008) exhibited dramatic inner-core structural variability in a 6-h rapid intensification and deepening event, from 0600 to 1200 UTC 23 July, prior to making landfall in southern Texas. Doppler radar data from the National Weather Service in Brownsville, Texas, indicated a dynamically active, highly asymmetric eyewall during this period. Prominent mesovortex and polygonal eyewall features were observed at azimuthal wavenumbers $m = 4$–7 from 0634 to 1234 UTC, and these features subsequently were observed to be at lower wavenumbers from 1307 to 1433 UTC. It has been shown here that the eyewall structural variability and a portion of the rapid deepening event (982–963 hPa) was most likely caused by barotropic instability of the eyewall PV ring and the ensuing PV mixing event, consistent with idealized dry, adiabatic and quasi-inviscid two-dimensional and three-dimensional modeling work. The rapid intensification event (70–85 kt) that occurred was not consistent with this idealized work, and may have resulted from a complicated nonlinear interaction between the dynamic instability (and subsequent PV advection) and diabatic/frictional effects in three dimensions. Further research on the modification of dry dynamic instability by diabatic and frictional effects appears warranted for the hurricane case. Overall, the results presented here indicate that internal vortex dynamics can be very important for rapid variability in tropical cyclone intensity.

*Acknowledgments.* EH acknowledges the support of the Office of Naval Research (ONR) Program Element (PE) 0602435N, and the NRL base program. BM acknowledges the support of the National Oceanographic Partnership Program (NOPP) through ONR Contract N00014-08-1-0250. WS acknowledges the support of NOPP through ONR Contract N00014-10-1-0145 as well as the National Science Foundation (NSF) through Grant ATM-0837932. The authors thank Jim Kossin and an anonymous reviewer for insightful comments that led to improvements in this manuscript. The authors also thank Scott Fulton, John Knaff, Mark DeMaria, Melinda Peng, and Jim Doyle for their comments and assistance.

REFERENCES

Chen, Y., and M. K. Yau, 2001: Spiral bands in a simulated hurricane. Part I: Vortex Rossby wave verification. *J. Atmos. Sci.,* **58,** 2128–2145.

DeMaria, M., M. Mainelli, L. K. Shay, J. A. Knaff, and J. Kaplan, 2005: Further improvements to the Statistical Hurricane Intensity Prediction Scheme (SHIPS). *Wea. Forecasting,* **20,** 531–543.

Hendricks, E. A., and W. H. Schubert, 2010: Adiabatic rearrangement of hollow PV towers. *J. Adv. Model. Earth Syst.,* **2,** 19 pp., doi:10.3894/JAMES.2010.2.8.

——, ——, R. K. Taft, H. Wang, and J. P. Kossin, 2009: Life cycles of hurricane-like vorticity rings. *J. Atmos. Sci.,* **66,** 705–722.

——, M. S. Peng, B. Fu, and T. Li, 2010: Quantifying environmental control on tropical cyclone intensity change. *Mon. Wea. Rev.,* **138,** 3243–3271.

Kossin, J. P., and M. D. Eastin, 2001: Two distinct regimes in the kinematic and thermodynamic structure of the hurricane eye and eyewall. *J. Atmos. Sci.,* **58,** 1079–1090.

——, and W. H. Schubert, 2001: Mesovortices, polygonal flow patterns, and rapid pressure falls in hurricane-like vortices. *J. Atmos. Sci.,* **58,** 2196–2209.

——, and ——, 2004: Mesovortices in Hurricane Isabel. *Bull. Amer. Meteor. Soc.,* **85,** 151–153.

——, B. D. McNoldy, and W. H. Schubert, 2002: Vortical swirls in hurricane eye clouds. *Mon. Wea. Rev.,* **130,** 3144–3149.

Kwon, Y., and W. M. Frank, 2005: Dynamic instabilities of simulated hurricane-like vortices and their impacts on the core structure of hurricanes. Part I: Dry experiments. *J. Atmos. Sci.,* **62,** 3955–3973.

Marks, F. D., R. A. Houze Jr., and J. F. Gamache, 1992: Dual-aircraft investigation of the inner core of Hurricane Norbert. Part I: Kinematic structure. *J. Atmos. Sci.,* **49,** 919–942.

Montgomery, M. T., V. A. Vladimirov, and P. V. Denissenko, 2002: An experimental study on hurricane mesovortices. *J. Fluid Mech.,* **471,** 1–32.

Nolan, D. S., and M. T. Montgomery, 2002: Nonhydrostatic, three-dimensional perturbations to balanced, hurricane-like vortices. Part I: Linearized formulation, stability, and evolution. *J. Atmos. Sci.,* **59,** 2989–3020.

——, and L. D. Grasso, 2003: Nonhydrostatic, three-dimensional perturbations to balanced, hurricane-like vortices. Part II: Symmetric response and nonlinear simulations. *J. Atmos. Sci.,* **60,** 2717–2745.

Pasch, R. J., and T. B. Kimberlain, 2011: Tropical cyclone report: Hurricane Dolly (AL042008) 20–25 July 2008. National Hurricane Center Archives, 19 pp. [Available online at http://www.nhc.noaa.gov/pdf/TCR-AL042008_Dolly.pdf.]

Reasor, P. D., M. T. Montgomery, F. D. Marks, and J. F. Gamache, 2000: Low-wavenumber structure and evolution of the hurricane inner core observed by airborne dual-Doppler radar. *Mon. Wea. Rev.,* **128,** 1653–1680.

Reynolds, R. W., and T. M. Smith, 1993: An improved real-time global sea surface temperature analysis. *J. Climate,* **6,** 114–119.

Roux, F., and N. Viltard, 2004: Structure and evolution of Hurricane Claudette on 7 September 1991 from airborne Doppler radar observations. Part I: Kinematics. *J. Atmos. Sci.,* **61,** 2105–2132.

Rozoff, C. M., J. P. Kossin, W. H. Schubert, and P. J. Mulero, 2009: Internal control of hurricane intensity: The dual nature of potential vorticity mixing. *J. Atmos. Sci.,* **66,** 133–147.

Schubert, W. H., M. T. Montgomery, R. K. Taft, T. A. Guinn, S. R. Fulton, J. P. Kossin, and J. P. Edwards, 1999: Polygonal eyewalls, asymmetric eye contraction, and potential vorticity mixing in hurricanes. *J. Atmos. Sci.,* **56,** 1197–1223.

Terwey, W. D., and M. T. Montgomery, 2002: Wavenumber-2 and wavenumber-*m* vortex Rossby wave instabilities in a generalized three-region model. *J. Atmos. Sci.,* **59,** 2421–2427.

Wang, Y., and C.-C. Wu, 2004: Current understanding of tropical cyclone structure and intensity changes—A review. *Meteor. Atmos. Phys.,* **87,** 257–278.

Yang, B., Y. Wang, and B. Wang, 2007: The effect of internally generated inner-core asymmetries on tropical cyclone potential intensity. *J. Atmos. Sci.,* **64,** 1165–1188.